Transcription factor EB improves ventricular remodeling after myocardial infarction by regulating the autophagy pathway

Cong Liu
The Seventh Affiliated Hospital Sun Yat-sen University
DaWang Zhou
The Seventh Affiliated Hospital Sun Yat-sen University
Qiang Zhang
The Seventh Affiliated Hospital Sun Yat-sen University
HongYan Wei
Sun Yat-sen University First Affiliated Hospital
YuanZheng Lu
The Seventh Affiliated Hospital Sun Yat-sen University
Bo Li
The Seventh Affiliated Hospital Sun Yat-sen University
HaoHong Zhan
Sun Yat-sen University First Affiliated Hospital
JingGe Cheng
The Seventh Affiliated Hospital Sun Yat-sen University
ChuYue Wang
The Seventh Affiliated Hospital Sun Yat-sen University
YiLin Yang
Sun Yat-sen University First Affiliated Hospital
ShuHao Li
Sun Yat-sen University First Affiliated Hospital
ChunLin Hu
Sun Yat-sen University First Affiliated Hospital
xiaoxing liao (liaoxx@mail.sysu.edu.cn)
The Seventh Affiliated Hospital Sun Yat-sen University https://orcid.org/0000-0002-0888-394X

Research Article

Keywords: TFEB, myocardial infarction, ventricular remodeling, autophagy

Posted Date: September 2nd, 2022

DOI: https://doi.org/10.21203/rs.3.rs-2009086/v1

Abstract

Background

Adverse left ventricular remodeling after myocardial infarction (MI) compromises cardiac function and increases heart failure risk. Till now, comprehension of the role transcription factor EB (TFEB) plays after MI is limited.

Objectives

The purpose of this study was to describe the effects of TFEB on cell death and fibroblast differentiation after MI.

Methods

AAV9 mediated up- and down-regulated TFEB expressions were generated in C57BL/6 mice two weeks before the MI modeling. Echocardiography, Masson, HE, Sirius red staining immunofluorescence, and wheat germ agglutinin staining were performed at 3 days, and 1, 2, and 4 weeks after MI modeling. Fibroblasts and myocytes collected from SD neonatal rats were transfected by adenovirus and siRNA, and cell counting kit-8 (CCK8), Cell Proliferation EdU Image (EDU), immunofluorescence, and Transwell assay were conducted. Myocardial fibrosis-related proteins and autophagy-related protein were identified by Western blot.

Results

The up-regulation of TFEB resulted in reduced myocardial cell death, delayed fibroblasts proliferation and its differentiation into myofibroblasts, and up-regulated expression of LC3B three days after MI. Similar results were observed in vitro studies. Meanwhile, a significant up-regulation of EF, decrease in the ratio of the infarction length, and decreased protein level of collagen III were observed four weeks after MI modeling. The over-expression of TFEB slowed down myofibroblast migration and resulted in a significant down-regulation of collagen I level in myofibroblasts.

Conclusions

TFEB demonstrated potential in improving cell death after MI by mediating autophagy and regulating fibroblast proliferation and transformation. Its molecular impacting mechanism deems further investigation.

1. Introduction

Acute myocardial infarction (AMI) is caused by hypoxia and ischemia, with high morbidity and mortality [1]. AMI often leads to heart failure (HF), which is the major risk patients have to face [2, 17]. Therefore,

effective treatment is needed to reduce the size of MI, preserve left ventricular (LV) function, and prevent HF in patients with AMI.

After AMI, extensive myocardial injury, impaired myocardial contractility, continuous activation of the neuroendocrine system, and remodeling of extracellular matrix (ECM) occur in the heart, which results in left ventricular remodeling (LVR). Adverse left ventricular remodeling affects cardiac function and increases the risk of HF [1]. Nowadays, myocardial remodeling is recognized as a complex process in response to cardiac overload and loss of functional myocardium, resulting in structural and functional disorders of the myocardium [16].

TFEB is one member of the microphthalmia-associated transcription factor E family and is actively involved in many cellular biological and pathological processes, including the occurrence and development of ischemia/reperfusion (I/R) injury. Studies showed that TFEB could decline I/R induced cardiomyocyte death by upregulating autophagy [6, 11]. Increased TFEB transcription activated by metformin and cilostazol could protect against I/R injury by regulating autophagy, lysosome, and apoptosis [10, 18].

In myocardial ischemia-reperfusion injury models, nicotinamide adenine dinucleotide (NAD+) could promote TFEB expression, alleviates lysosomal dysfunction, and alleviates myocardial I/R induced microvascular injury [20]. After MI, Fibroblasts will proliferate and differentiate into myofibroblasts. Myofibroblasts express the contractile proteins α-smooth muscle actin (α-SMA) and embryonic smooth muscle myosin, exhibit an extended endoplasmic reticulum, and secrete abundant matrix proteins to generate collagen scars [4]. Adverse fibrosis will lead to myocardial stiffness, diastolic and systolic dysfunction, and eventually the development of HF [14]. Till now, whether TFEB was involved in the fibrosis process after MI remains unclear. Thus, we designed this study to systematically evaluate the impacts of TFEB on the pathology processes of autophagy, ventricular remodeling, and fibrosis after MI.

2. Materials And Methods

2.1 Reagents

TGF-ß1 was purchased from Sino Biological (Beijing, China). The adeno-associated virus 9 (AAV9) was purchased from Weizhen Technology Co., LTD. (Shandong, China). In the TFEB-overexpression mice built by adeno-associated virus, gene ID: NM_011549, vector: PAV-CMV-P2A-GFP (CMV promoter), virus titer: 3.84 x 10^{13} μg/ml; AAV9-NC was GFP (CMV promoter) control adeno-associated virus with a titer of 8.02×10^{13} μg/mL. In the AAV9-shTFEB mice with TFEB expression down-regulated by AAV9 4in1shRNA, gene ID: NM_011549, vector: PAV-4IN1shrNA-GFP; primer design: positive CGGCAGTACTATGACTATGA, reverse: GCCGTCATGATACTGATACTA; Virus titer: 2.22×10^{13} μg/mL; AAV9-sh-TFEB virus was AAV9-U6-GFP control adeno-associated virus inserted with nonsense sequence, and the virus titer was 4.74×10^{13} μg/ mL. All the dilution virus titer was 1×10^{13} ug/ml, and the dose was 10μl for each mouse. The adenovirus used in the in vitro study was purchased from Hanheng Biology (Shanghai, China). Ad-TFEB

was HBAD-TFeb-EGFP overexpressed virus, gene sequence number: NM_001025707. Ad-Gfp was used as a control virus with HBAD-EGFP overexpression. The multiplicity of cellular infection (MOI) of the virus infection complex in the 6-well plate was 30, with an adenovirus volume of 10μL. The MOI of the virus infection complex in the 24-well plate was 30, with an adenovirus volume of 3μL. The siRNAs were used to reduce TFEB expression, with Si-NC serving as control. The target sequence of siRNAs: GCAGTCTCAGCATCAGAAA.

2.2 Animals and MI modeling

We used male mice to establish a stable MI model considering that Estrogen has shown a protective effect against pathological hypertrophic remodeling in pressure-overload. [3, 13]. Two-month-old wild-type male C57BL/6 mice (20-30g) were purchased from the Animal Experimental Centre of Jicui Yaokang Biotechnology Co. LTD. (Jiangsu, China). All mice were fed in the SPF animal laboratory at the Animal Center of Sun Yat-Sen University, Guangzhou, China, with free access to standard laboratory food and water. Thirty mice were equally randomized into five groups: Sham group, AAV9-TFEB group, AAV9-NC group, AAV9-shTFEB group, and AAV9-shNC group. The AAV9-NC and AAV9-sh-NC group served as controls of the AAV9-TFEB and AAV9-sh-TFEB groups, respectively. All mice were pretreated with myocardial multipoint injection of Adeno-associated virus 9 (AAV9) for two weeks before the MI modeling. All the dilution virus titer was 1×10^{13} ug/ml, and the dose was 10μl for each mouse. After 14 days of feeding, the anterior descending branch of the mice's left coronary artery (LAD) was permanently ligated to set up the MI model. The surgery was conducted under the anesthetization of 50 mg/kg intraperitoneally injected pentobarbital sodium (Sigma) and endotracheal intubation. For mice in the Sham group, the chest was surgically opened without LAD ligation. Echocardiography was performed every day for 28 days. The mice were anesthetized and sacrificed by cervical dislocation at different time points after MI or sham operation. Hearts were collected and stored at −80 °C for the next step measurements. The flowchart of this experiment is illustrated in figure 2A.

2.3 Echocardiography

Echocardiography was performed on the VisualSonics machine Vevo 3100. Mice were anesthetized by Isoflurane (Rayward Life Technology Co., LTD., Shenzhen, China). Mouse chests were hair-shaved, and the animals were positioned on a warm cushion. Left ventricular ejection fraction (LVEF) was measured in M-mode short-axis at the level of papillary muscles.

2.4 Masson staining and HE staining

The infarction regions of left ventricular tissues were fixed in 4% paraformaldehyde (Servicebio, Wuhan, China) for at least 24 hours, then embedded in paraffin. Sections of 3-6 μm thickness were stained following the Masson trichrome standard protocol (BP028, Biossci, China) and the HE staining protocol (BP092, Biossci, China). In Masson-stained sections, myocardial cells appear red, while collagen appears blue. In HE-stained sections, the cytoplasm was dyed pink, and the cell nucleus was stained blue.

2.5 Sirius red staining

The infarction regions of left ventricular tissues were fixed in 4% paraformaldehyde (Servicebio, Wuhan, China) for at least 24 hours before being embedded in paraffin. Sections of 3-6 μm thickness were stained by the Picro Sirius Red Stain Kit (Phygene, China) following the official guidelines. After staining, collagen I appears orange, and Collagen III appears green.

2.6 Wheat germ agglutinin staining

The whole heart was fixed in 4% paraformaldehyde (Servicebio, Wuhan, China) and embedded in paraffin. Sections of 3-6 μm thickness were stained with fluorescein isothiocyanate-conjugated wheat germ agglutinin (WGA-FITC, MP6325, MKbio, China) to assess the cardiomyocyte cross-sectional area in myocardial sections. The results of WGA staining were observed under a confocal microscope (LSM 880, Zeiss, Germany).

2.7 Immunofluorescence analysis

An immunofluorescence assay was performed to detect the expression and distribution of α-smooth muscle actin (α-SMA; 1:8000; Abcam) in the differentiated myofibroblasts, and vimentin (1:200; Abways) was used as an internal control tagging undifferentiated fibroblasts. TFEB protein was tagged by TFEB (1:200; Absin) antibody. In the immunofluorescence staining, the myocytes were marked by ACTA (1:200; Abcam) and the nuclei were counterstained with 0.5 μg/mL 4',6-diamidino-2-phenylindole (DAPI; 1:500, Solarbio). The result of staining was imaged using an immunofluorescence microscope (BX53, Olympus).

2.8 Protein extraction and Western blotting

Proteins in Cells or mice organs were extracted following standard procedures using the protein extraction reagents of Ripa (Millipore), PMSF (CST), a protease inhibitor (Roche), and phosphatase inhibitor (Roche). The protein concentration was tested by the BCA Quantitative Kit (Thermo). Equal amounts of total protein (30 μg) were separated by 8% SDS-PAGE gels and transferred to PVDF membranes. After being blocked in 5% skim milk for one hour, the membranes were subsequently incubated with primary antibodies at 4°C overnight and then the secondary antibodies at room temperature for one hour. The membranes were then exposed to chemiluminescence developing agents. The antibodies used in this process were as followed: mouse anti- Collagen III (NBP1-05119, Novus), rabbit anti- Collagen I (NB600-408, Novus), rabbit anti-LC3B (2775s, CST), rabbit anti-TFEB (abs131998, Absin), rabbit anti-Lamin-B1 (NBP2-48966, Novus), and rabbit anti-GAPDH (sc-166545, SANTACRUZ). GAPDH was used as an internal control.

2.9 Myocytes isolation and building of Oxygen Glucose Deprivation Model

Primary neonatal rat myocytes were isolated from the heart of 1- to 3-day-old SD rats, digested with 0.05% collagenase type II and trypsin, and dispersed via gentle mechanical attrition. After centrifugation,

cells were cultured in DMEM/F-12 (Gibco), supplemented with 10% newborn calf serum (Gibco), 50 U/mL penicillin, 50μg/mL streptomycin in a 37°C, 5% CO_2 incubator with assisted circulation. On day four, absorbed and discarded the culture medium gently, washed the wells using PBS (five minutes twice), and then added 1.5 mL sugar-free medium per well immediately. Oxygen Glucose Deprivation (OGD) modeling: The culture plate was placed in a sealed cell culture box with a ventilation tube, maintained with 95% N_2+5% CO_2 (flow rate kept at 0.2L /min). After 15 minutes of ventilation, the ventilation tube was closed to ensure the box was completely filled with mixed gas. The oxygen concentration at this time was 0.1%. Hypoxia was induced by incubation under 37 ℃.

2.10 Myocardial fibroblasts isolation and culture

Primary neonatal rat fibroblasts were isolated from the heart of 1- to 3-day-old SD rats. The fibroblasts were distinguished from myocytes by a shorter adherent time to the well. After centrifugation, cells were cultured in DMEM/F-12 (Gibco), supplemented with 10% fetal bovine serum (Gibco), 50 U/mL penicillin, 50μg/mL streptomycin in a 37°C, 5% CO2 incubator in NHC key Laboratory of Assisted Circulation. The second generation of the CFs was used for the experiments. Cells were treated with virus or siRNA and were cultured in a serum-free medium at least 24 hours before being treated with 5ng/ml TGF-ß1 for 12 hours.

2.11 Cell counting kit-8 (CCK-8) assay and EDU assay

CFs were transferred into 24-well plates. Cells were treated with Virus or siRNAs and were cultured for at least 24 hours in a serum-free medium before being treated with 5ng/ml TGF-ß1 for 12 hours. The proliferation of cells was determined by a CCK-8 kit (MCE) and an EDU kit (KTA2030, Abbkine). The optical density (OD) of each well was examined at 450 nm using a microplate reader (Thermo Scientific). The proliferation rate was calculated by the results of OD and fluorescence.

2.12 Transwell assay

Transwell assay was performed on the second generation of the CFs. Cells were treated with Virus or siRNAs and were cultured for at least 24 hours in a serum-free medium before being co-incubated with 5ng/ml TGF-ß1 and the Transwell inserts for 12 hours. CF cells were plated on the upper side of the chambers. After 12 hour's incubation, the cells that migrated to the lower side of the chambers were counted through DAPI staining.

2.13 TUNEL assay

After adenovirus transductions, apoptotic cells in each well (24-well plates) were visualized using the TUNEL assay following the manufacturer's instructions (Roche). The results of TUNEL assay were observed and imaged under a confocal microscope (LSM 880, Zeiss, Germany).

2.14 Statistical analysis

All data were presented as the means ± standard deviation (SD). The results were analyzed by one-way analysis of variance (ANOVA) or the Student *t*-test, and a $p < 0.05$ was considered to be statistically significant.

3. Results

3.1 The expression of autophagy-related protein and extracellular matrix after MI molding

We evaluated the heart tissues at different times after MI modeling. Western blotting was used to evaluate the expression of key proteins associated with ECM, such as collagen I and collagen III. Sirius red staining could also distinguish the distribution of collagen I and collagen III. Collagen III increased slowly and reached a peak at four weeks. These results suggest that the synthesis and secretion of ECM after MI are dynamic processes (Figure 1A-B). Autophagy-related protein LC3B-II began to increase three days after MI and decrease one week after MI (Figure 1B). We also found that TFEB expressed most one week after MI (Figure 1B). To explain the decline of collagen I one week after MI, we conducted HE and immunofluorescence stains. The images showed fibroblasts died abundantly one week after MI (Figure 1C).

3.2 Extent of MI and systolic function of heart

We observed that the impacts of TFEB varied significantly over time. Immunofluorescence staining verified TFEB expression in the cytoplasm and nucleus (Figure 2B). Four weeks after MI, AAV9-TFEB group had smaller hearts and LV volume (Figure 2C). The survival curves showed that mice died in succession after the MI modeling, and AAV9-shTFEB group had a higher mortality rate (Figure 2D). The echocardiography after three and four weeks of MI modeling confirmed a higher EF value in the AAV9-TFEB group (Figure 2E), and Masson staining showed the infarcted area in the left ventricular got increasingly thinner. In the AAV9-TFEB group, the ratio of infarcted length to left ventricle length decreased four weeks after modeling, and the ratio of the infarcted area also decreased two weeks after modeling (Figure 2F-H). These results suggest that TFEB alleviated infarction extension and protects the systolic function of the heart. Those explained the fewer mice deaths in the TFEB over-expression group.

3.3 TFEB impacts cell autophagy induced by MI modeling.

TFEB influenced cell death by regulating the autophagy process. Since TFEB and autophagy-related protein LC3B changed over time after MI, we explored their correlations. TFEB transfected into the nucleus three days after MI modeling in mice (Figure 3A). HE-stained cross-sections of the ventricles showed that myocardial cells in the AAV9-TFEB group had a smaller death area compared with the AAV9-NC group (Figure 3B). AAV9-TFEB group had a higher LC3B expression than the AAV9-NC group three days after MI modeling (Figure 3C). These results suggested that TFEB could improve autophagy and decrease cell death.

3.4 TFEB Affected the differentiation of fibroblasts three days after MI modeling.

Two to four days after modeling, fibroblasts activated by the stimulation of inflammatory cytokines began to proliferate and produce ECM [9]. We tested the proliferation and differentiation of fibroblasts three days after the modeling. Immunofluorescence staining highlighted vimentin-tagged fibroblasts and α-SMA-tagged myofibroblasts. AAV9-TFEB group had fewer fibroblasts and a lower myofibroblasts ratio than the AAV9-NC group. The AAV9-shTFEB group had more fibroblasts and a higher myofibroblasts ratio than the AAV9-shNC group. These results suggest that TFEB delayed fibroblast differentiation into myofibroblasts (Figure 4A).

3.5 TFEB Regulates myocardial hypertrophy and extracellular matrix synthesis and transformation in vivo

Due to myocardial cell death, the infarcted area could not contract perfectly; thus, the surviving cardiomyocytes become hypertrophy as time prolongs (Figure 5A-B). AAV9-shTFEB group showed a larger myocyte area than the AAV9-shNC group. WGA staining showed that TFEB down-regulation was associated with more severe cardiac hypertrophy (Figure 5C). As revealed by the Sirius red staining and western blot, a large amount of collagen III was synthesized four weeks after MI modeling. At the same time, the expression of collagen I decreased (Figure 5D). AAV9-TFEB group had a lower concentration of collagen III than the AAV9-NC group. (Figure 5E).

3.6 TFEB's impact on Myocardial Autophagy and Apoptosis in OGD Model.

OGD time of rat myocardial cells was measured by CCK-8 assay. Six hours was chosen as the appropriate test time with nearly 50% of cell death (Figure 6A). The Ad-TFEB group showed better cell viability than the Ad-Gfp group. TFEB improved the viability of rat myocardial cells six hours after OGD (Figure 6B). Myocardial cells were tagged by ACTA in Immunofluorescence staining. TFEB was over-expressed in the nucleus of myocardial cells in the OGD model (Figure 6C-D). TUNEL staining revealed that AAV9-TFEB group alleviated myocardial cell apoptosis after OGD when compared to the AAV9-NC group (Figure 6E). The Ad-TFEB group had higher expression of LC3B than the Ad-Gfp group (Figure 6F). These results suggested that TFEB improved autophagy and decreased cell apoptosis.

3.7 Effects of TFEB on cardiac fibroblasts during fibrosis model in vitro

TGF-ß1 was used to simulate fibroblast proliferation and its differentiation into myofibroblasts. The adenovirus used in the in vitro study upregulated TFEB expression in CFs, and Si-RNA downregulated it. In rat CFs, fibroblasts were tagged by vimentin in the Immunofluorescence staining (Figure 7A). CFs cells were co-incubated with TGF-β1 of different concentrations including 2 ng/mL, 5 ng/mL, 8 ng/mL, 10 ng/mL, and 20 ng/mL for different duration including 6, 12, 24, 36, and 48 hours. CCK-8 results indicated that low concentration TGF-β1 promoted CFs proliferation, while high concentrations inhibited (Figure 7B). The Ad-TFEB group showed no statistical differences from the Ad-Gfp group in the CCK-8 test and EDU test after 12 hours of co-incubation with 5ng/ml TGF-β1 (Figure 7C-D). The Ad-TFEB group had a lower cell migration than the Ad-Gfp group (Figure 7E). Western blot results indicated that 12-hour TGF-β1 stimulation increased collagen I expression. The Si-TFEB group had a higher collagen I expression than the Si-NC group (Figure 7F).

Discussion

Cardiac repair after MI consists of three phases: a pro-inflammatory phase (1-3 days after MI), an anti-inflammatory repair or proliferative phase (4-7 days after MI), and a maturation phase (7 days after MI) [12, 15, 19]. The pro-inflammatory phase aims to remove cellular debris from the ischemic infarct area. This inflammatory process is usually destructive and leads to excessive death of surviving cardiomyocytes, affecting the final infarct size [21]. Then, an elaborate interaction between immune cells, cardiomyocytes, and the stroma simulates the transition to the anti-inflammatory repair phase. During this repair phase, acute inflammatory responses are down-regulated, myocardial damage is relieved, and the wound heals and scars to prevent heart rupture. The inflammatory and fibrotic activity return to be quiescent when it reaches the maturation phase. Continuous monitoring of heart tissues after MI showed that autophagy and fibrosis started on day three; thus, day three was selected as the first observation point. TFEB improved autophagy and inhibited cell apoptosis in the OGD model. In our in vivo studies, TFEB promoted autophagy and inhibited cell death. TFEB alleviated infarction extension and protected the systolic function of the heart. WGA staining showed that TFEB down-regulation was associated with severe cardiac hypertrophy. Those might explain the lower mortality of mice in the AAV9-TFEB group.

As the final stage of MI repair, the maturation phase is associated with remodeling of the ECM which commonly lasts for several months. Scar maturation is a process intertwining the reduction in infarct fibroblast numbers [4], the differentiation of fibroblast into myofibroblast, the apoptosis of activated fibroblasts, the and expression of matrix-specific proteins [5]. The purpose of scarring is to prevent myocardial rupture and deterioration of partially restricted cardiac function.

After MI, the LV undergoes geometric and functional changes, with thinning and dilation of the infarcted area and hypertrophy of the other areas [12]. Thus, LV remodeling predicts a poor clinical prognosis. Main pathological features of ventricular remodeling include extensive fibrosis, pathological cardiomyocyte hypertrophy, and cardiomyocyte apoptosis. The balance between excessive synthesis and degradation of myocardial fibrotic collagen is critical for maintaining myocardial ECM homeostasis. Thus, we continuously monitored the fibrosis process after MI modeling and probed the role of TFEB during LVR in an attempt to improve the prognosis of MI. Two to four days after injury, fibroblasts activated by the stimulation of inflammatory cytokines began to proliferate and produce ECM [9]. The transformation from fibroblasts to myofibroblasts mainly occurred four to seven days after MI [5]. Myofibroblasts are characterized by the extensive endoplasmic reticulum, the expression of α-smooth muscle actin (α-SMA), and the synthesis of matricellular proteins [7]. Thus, we detected the myofibroblasts by α-SMA staining. In our study, TFEB inhibited fibroblastdifferentiation into myofibroblasts as early as three days after MI. After MI, collagen I expressed anterior to collagen III. TFEB inhibited collagen I expression in the fibrosis model in vivo. Four weeks after MI, TFEB decreased collagen III synthesis, but did not show an impact on the collagen I concentration in mice. This might be because collagen I expression was very low. TFEB inhibited cell migration in the fibrosis model. Besides, TGF-β1 showed an inhibitory effect on the expression of TFEB in the in vivo study. Unveiling the impacting mechanisms of TFEB in the fibrosis process requires further investigations.

Ali et al. [8] noticed in an ischemia-reperfusion (IR) mice model that, four weeks after MI, the average EF of mice recovered in the group of inducible macrophage-specific over-expression of transcription factor EB (Mϕ-TFEB), significantly higher than that in the control group. In addition, LV end-diastolic volume (EDV) was significantly smaller in the over-expression group, whereas the area-at-risk was very similar between the two groups. These results showed that Mϕ-TFEB expression could improve ventricular function after IR injury, and TFEB in macrophages played a role in ventricular remodeling after MI by mediating the inflammatory response. However, all the results were observed in an ischemia-reperfusion model instead of a MI model, and the ventricular remodeling in this study might have been mild. Meanwhile, inflammatory cells might not be the most important effector cells in late-stage ventricular remodeling. Since the pathophysiology after MI is a dynamic process, continuous monitoring is necessary. Therefore, our study focused on the MI model and conducted continuous monitoring of the hearts at different time points after the MI modeling in mice. Furthermore, the virus transfection method in this study guaranteed an optimum transfection rate in the heart cells.

The main defect of this study is that TFEB only demonstrated an inhibition effect on fibroblast migration and collagen I secretion in the in vitro studies. This might have been caused by the low concentration of TGF-β1 and the short inoculation time, which as a result only simulated the early stage of fibrosis. Thus, future studies with longer co-inoculation time with higher levels of TGF-β1 might provide a more comprehensive understanding of TFEB's impacts on the proliferation of fibroblasts.

Declarations

Funding Information

This study was supported by the National Natural Science Foundation of China (Grant Number: 81571865), The National Science Fund for Distinguished Young Scholars (Grant Number: 81901931), the Basic and Applied Basic Research Fund of Guangdong Province (2020A1515010120 and 2020A1515110827), and the Shenzhen Science and Technology Project (No. JCYJ20160608142215491 and JCYJ20190809150817414).

Conflicts of interest

The authors have no conflicts of interest to declare that are relevant to the content of this article.

Ethical Approval

In this study, all animal experiments were approved by the Institutional Animal Care and Use Committee of the Sun Yat-Sen University (SYSU-IACUC-2021-000659).

Abbreviations

AAV9, Adeno-associated virus 9; α-SMA, α-smooth muscle actin; CCK8, cell counting kit-8; ECM, extracellular matrix; EDU, Cell Proliferation EdU Image; HF, heart failure; I/R, ischemia/reperfusion; LAD,

anterior descending branch of the left coronary artery; LV, left ventricular; MI, myocardial infarction; OGD, Oxygen Glucose Deprivation; TFEB, transcription factor EB.

Code availability

Not applicable

Author Contributions

C.L., and D.Z. interpreted the data, designed the analyses, and contributed to the manuscript. Q.Z., H.Z., and S.L. contributed to data acquisition. B.L., Y.L., Y.Y., J.C., C.W., and H.W. contributed to the data interpretation. C.H. and X.L. are the guarantors of this work and take responsibility for the integrity and accuracy of the data. All authors have read and agreed to the published version of the manuscript.

Consent to participate

Not applicable

Consent for publication

All authors gave their consent for publication.

References

1. Azevedo PS, Polegato BF, Minicucci MF, Paiva SA, Zornoff LA. Cardiac Remodeling: Concepts, Clinical Impact, Pathophysiological Mechanisms and Pharmacologic Treatment. Arq Bras Cardiol. 2016;106:62–9. doi:10.5935/abc.20160005.
2. Bahit MC, Kochar A, Granger CB. Post-Myocardial Infarction Heart Failure. JACC Heart Fail. 2018;6:179–86. doi:10.1016/j.jchf.2017.09.015.
3. Cao J, Zhu T, Lu L, Geng L, Wang L, Zhang Q, Yang K, Wang H, Shen W. Estrogen induces cardioprotection in male C57BL/6J mice after acute myocardial infarction via decreased activity of matrix metalloproteinase-9 and increased Akt-Bcl-2 anti-apoptotic signaling. Int J Mol Med. 2011;28:231–7. doi:10.3892/ijmm.2011.681.
4. Frangogiannis NG, Michael LH, Entman ML. Myofibroblasts in reperfused myocardial infarcts express the embryonic form of smooth muscle myosin heavy chain (SMemb). Cardiovasc Res. 2000;48:89–100. doi:10.1016/s0008-6363(00)00158-9.
5. Fu X, Khalil H, Kanisicak O, Boyer JG, Vagnozzi RJ, Maliken BD, Sargent MA, Prasad V, Valiente-Alandi I, Blaxall BC, Molkentin JD. Specialized fibroblast differentiated states underlie scar formation in the infarcted mouse heart. J Clin Invest. 2018;128:2127–43. doi:10.1172/JCI98215.
6. Godar RJ, Ma X, Liu H, Murphy JT, Weinheimer CJ, Kovacs A, Crosby SD, Saftig P, Diwan A. Repetitive stimulation of autophagy-lysosome machinery by intermittent fasting preconditions the myocardium to ischemia-reperfusion injury. Autophagy. 2015;11:1537–60. doi:10.1080/15548627.2015.1063768.

7. Hinz B. The myofibroblast: paradigm for a mechanically active cell. J Biomech. 2010;43:146–55. doi:10.1016/j.jbiomech.2009.09.020.
8. Javaheri A, Bajpai G, Picataggi A, Mani S, Foroughi L, Evie H, Kovacs A, Weinheimer CJ, Hyrc K, Xiao Q, Ballabio A, Lee JM, Matkovich SJ, Razani B, Schilling JD, Lavine KJ, Diwan A. (2019) TFEB activation in macrophages attenuates postmyocardial infarction ventricular dysfunction independently of ATG5-mediated autophagy. JCI Insight 4 doi:10.1172/jci.insight.127312.
9. Kurose H. (2021) Cardiac Fibrosis and Fibroblasts. Cells 10 doi:10.3390/cells10071716.
10. Li J, Xiang X, Xu Z. Cilostazol protects against myocardial ischemia and reperfusion injury by activating transcription factor EB (TFEB). Biotechnol Appl Biochem. 2019;66:555–63. doi:10.1002/bab.1754.
11. Ma X, Liu H, Murphy JT, Foyil SR, Godar RJ, Abuirqeba H, Weinheimer CJ, Barger PM, Diwan A. Regulation of the transcription factor EB-PGC1alpha axis by beclin-1 controls mitochondrial quality and cardiomyocyte death under stress. Mol Cell Biol. 2015;35:956–76. doi:10.1128/MCB.01091-14.
12. Ong SB, Hernandez-Resendiz S, Crespo-Avilan GE, Mukhametshina RT, Kwek XY, Cabrera-Fuentes HA, Hausenloy DJ. Inflammation following acute myocardial infarction: Multiple players, dynamic roles, and novel therapeutic opportunities. Pharmacol Ther. 2018;186:73–87. doi:10.1016/j.pharmthera.2018.01.001.
13. Patten RD, Pourati I, Aronovitz MJ, Baur J, Celestin F, Chen X, Michael A, Haq S, Nuedling S, Grohe C, Force T, Mendelsohn ME, Karas RH. 17beta-estradiol reduces cardiomyocyte apoptosis in vivo and in vitro via activation of phospho-inositide-3 kinase/Akt signaling. Circ Res. 2004;95:692–9. doi:10.1161/01.RES.0000144126.57786.89.
14. Prabhu SD, Frangogiannis NG. The Biological Basis for Cardiac Repair After Myocardial Infarction: From Inflammation to Fibrosis. Circ Res. 2016;119:91–112. doi:10.1161/CIRCRESAHA.116.303577.
15. Ruparelia N, Chai JT, Fisher EA, Choudhury RP. Inflammatory processes in cardiovascular disease: a route to targeted therapies. Nat Rev Cardiol. 2017;14:133–44. doi:10.1038/nrcardio.2016.185.
16. van der Bijl P, Abou R, Goedemans L, Gersh BJ, Holmes DR Jr, Ajmone Marsan N, Delgado V, Bax JJ. Left Ventricular Post-Infarct Remodeling: Implications for Systolic Function Improvement and Outcomes in the Modern Era. JACC Heart Fail. 2020;8:131–40. doi:10.1016/j.jchf.2019.08.014.
17. Velagaleti RS, Pencina MJ, Murabito JM, Wang TJ, Parikh NI, D'Agostino RB, Levy D, Kannel WB, Vasan RS. Long-term trends in the incidence of heart failure after myocardial infarction. Circulation. 2008;118:2057–62. doi:10.1161/CIRCULATIONAHA.108.784215.
18. Wang Y, Yang Z, Zheng G, Yu L, Yin Y, Mu N, Ma H. Metformin promotes autophagy in ischemia/reperfusion myocardium via cytoplasmic AMPKalpha1 and nuclear AMPKalpha2 pathways. Life Sci. 2019;225:64–71. doi:10.1016/j.lfs.2019.04.002.
19. Westman PC, Lipinski MJ, Luger D, Waksman R, Bonow RO, Wu E, Epstein SE. Inflammation as a Driver of Adverse Left Ventricular Remodeling After Acute Myocardial Infarction. J Am Coll Cardiol. 2016;67:2050–60. doi:10.1016/j.jacc.2016.01.073.

20. Zhang YJ, Zhang M, Zhao X, Shi K, Ye M, Tian J, Guan S, Ying W, Qu X. NAD(+) administration decreases microvascular damage following cardiac ischemia/reperfusion by restoring autophagic flux. Basic Res Cardiol. 2020;115:57. doi:10.1007/s00395-020-0817-z.
21. Zhao ZQ, Velez DA, Wang NP, Hewan-Lowe KO, Nakamura M, Guyton RA, Vinten-Johansen J. Progressively developed myocardial apoptotic cell death during late phase of reperfusion. Apoptosis. 2001;6:279–90. doi:10.1023/a:1011335525219.

Figures

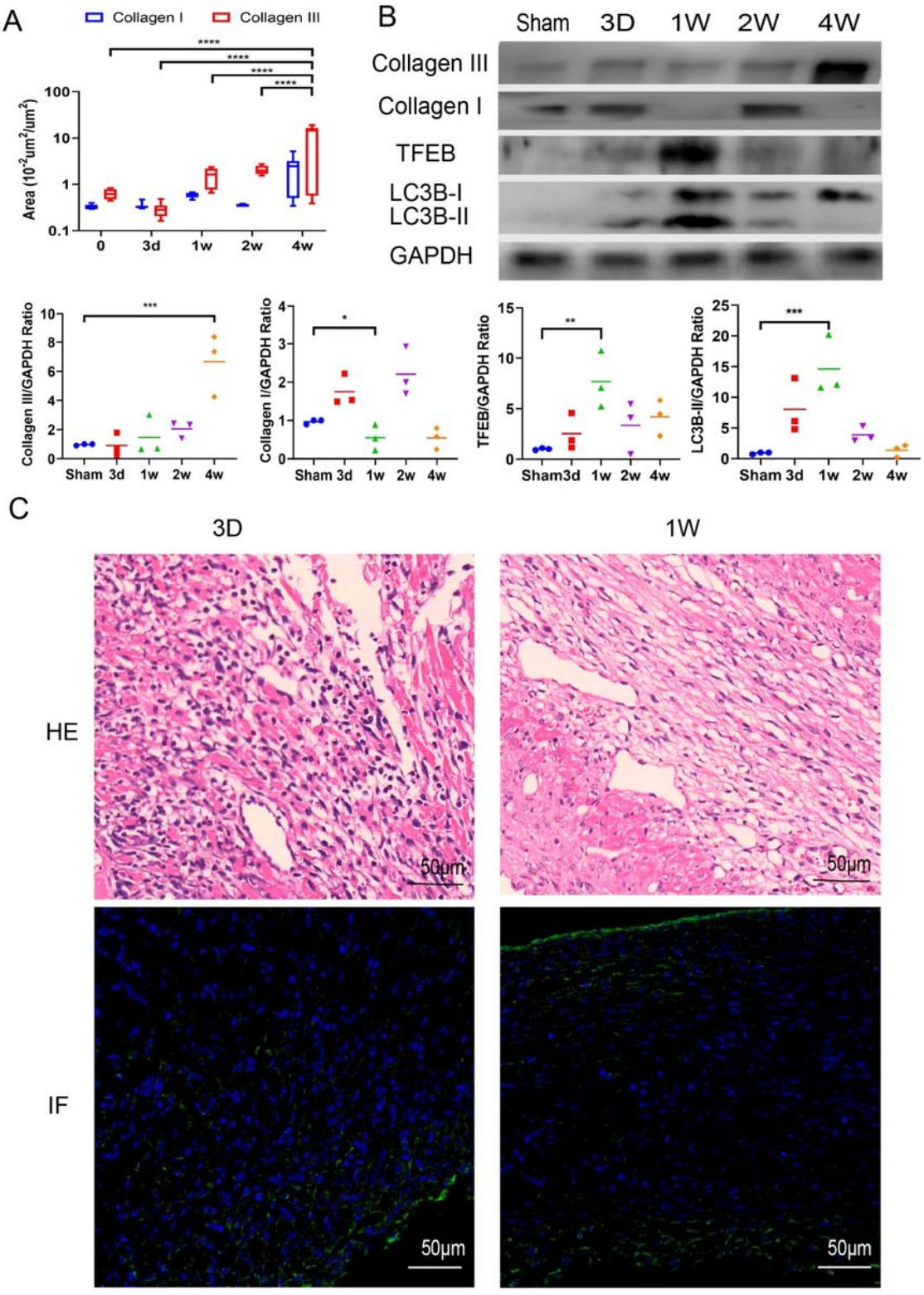

Figure 1

Expression of autophagy-related proteins and ECM in mice at different time points after MI surgery. (A) The Sirius red staining results of Collagen I, Collagen III in MI areas at different time points (****: $p <$ 0.0001)(n=3). (B) The Western blotting results of Collagen I, Collagen III, and LC3B in infarcted areas at different time points(n=3). (C) Representative HE and immunofluorescence images of vimentin (green) in

the infarction area from MI mouse hearts(n=3). Scale bars represent 50 mm. The results were presented as mean ± standard deviation (*: $p < 0.05$, ***: $p < 0.001$).

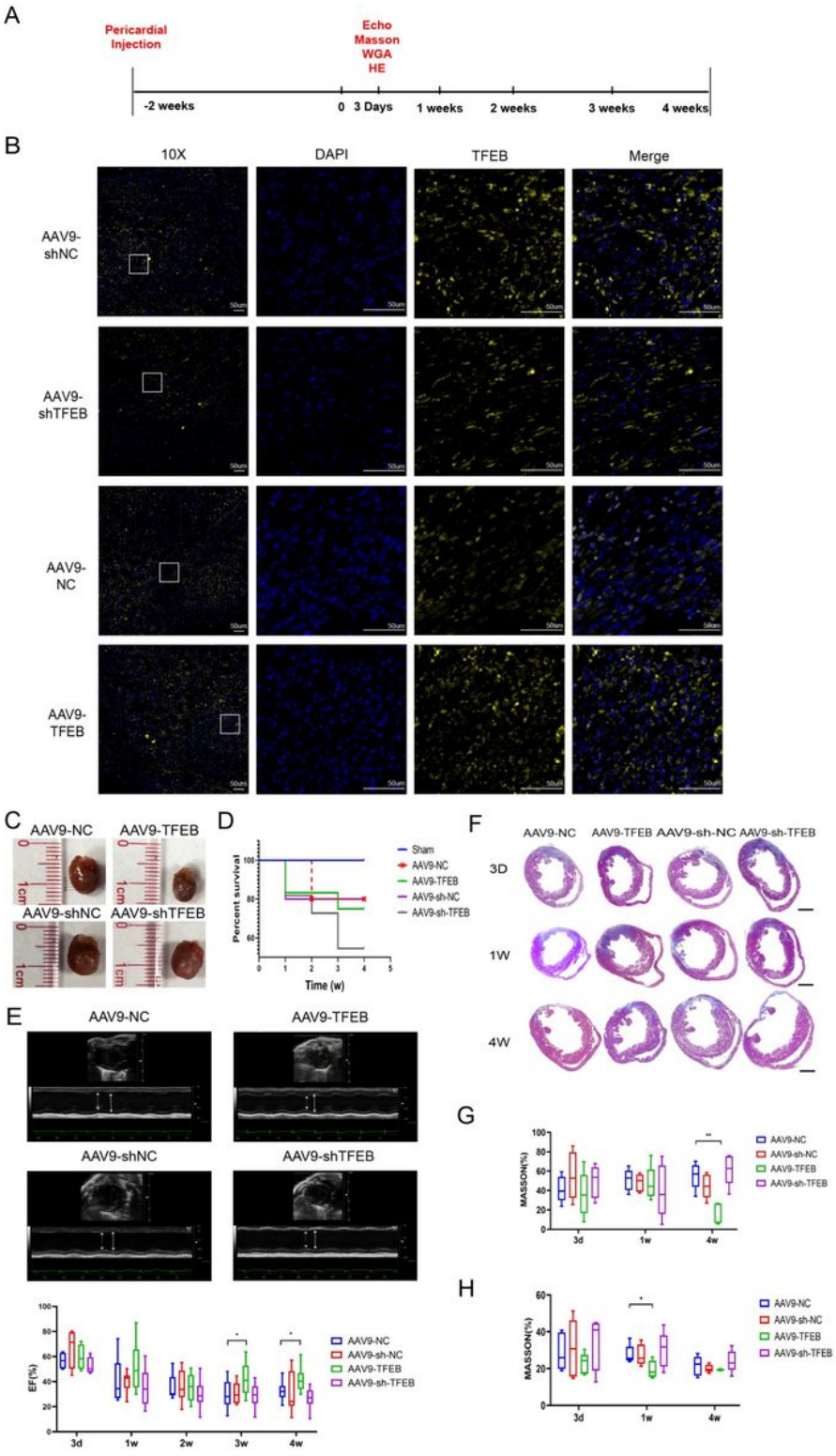

Figure 2

TFEB Reduced MI Area in mice. (A) Procedure of mice MI modeling after injecting with AAV9. (B) Confocal image of the Immunofluorescence staining of TFEB (yellow) of mouse heart three days after MI

modeling(n=3). Scale bars represent 50 mm. (C) Image of MI mouse hearts under natural light(n=6). (D) Survival curves of mice in each group(n=6). (E) Echocardiography of the mice and the qualified EF ratios in each group (*: $p < 0.05$)(n=6). (F) MI areas display in the Masson-stained mouse hearts(n=3). Scale bars represent 1 mm. (G) Ratios of MI length to the ventricular cavity (**: $p < 0.01$)(n=3). (H) Ratios of MI areas to the ventricular cavity (*: p <0 .05)(n=3).

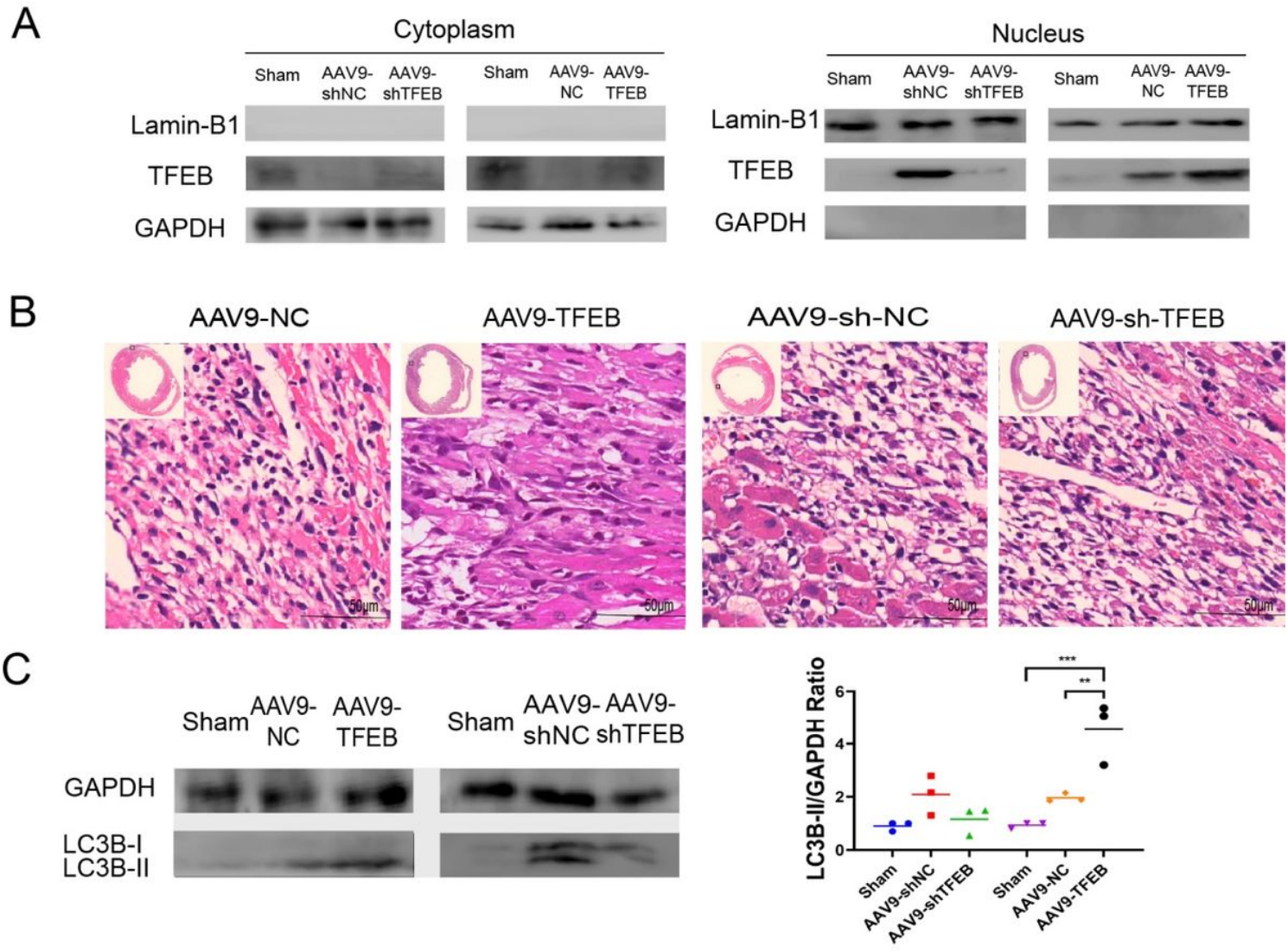

Figure 3

TFEB's effect on cell autophagy three days after MI modeling. (A) Western blot of TFEB expression in the nucleus and cytoplasm in infarcted areas. (B) Cross-sections of HE-stained ventricles display the dead myocardial cells(n=3). (C) The expressions of autophagy-related proteins in infarcted areas were detected using Western blot(n=3).

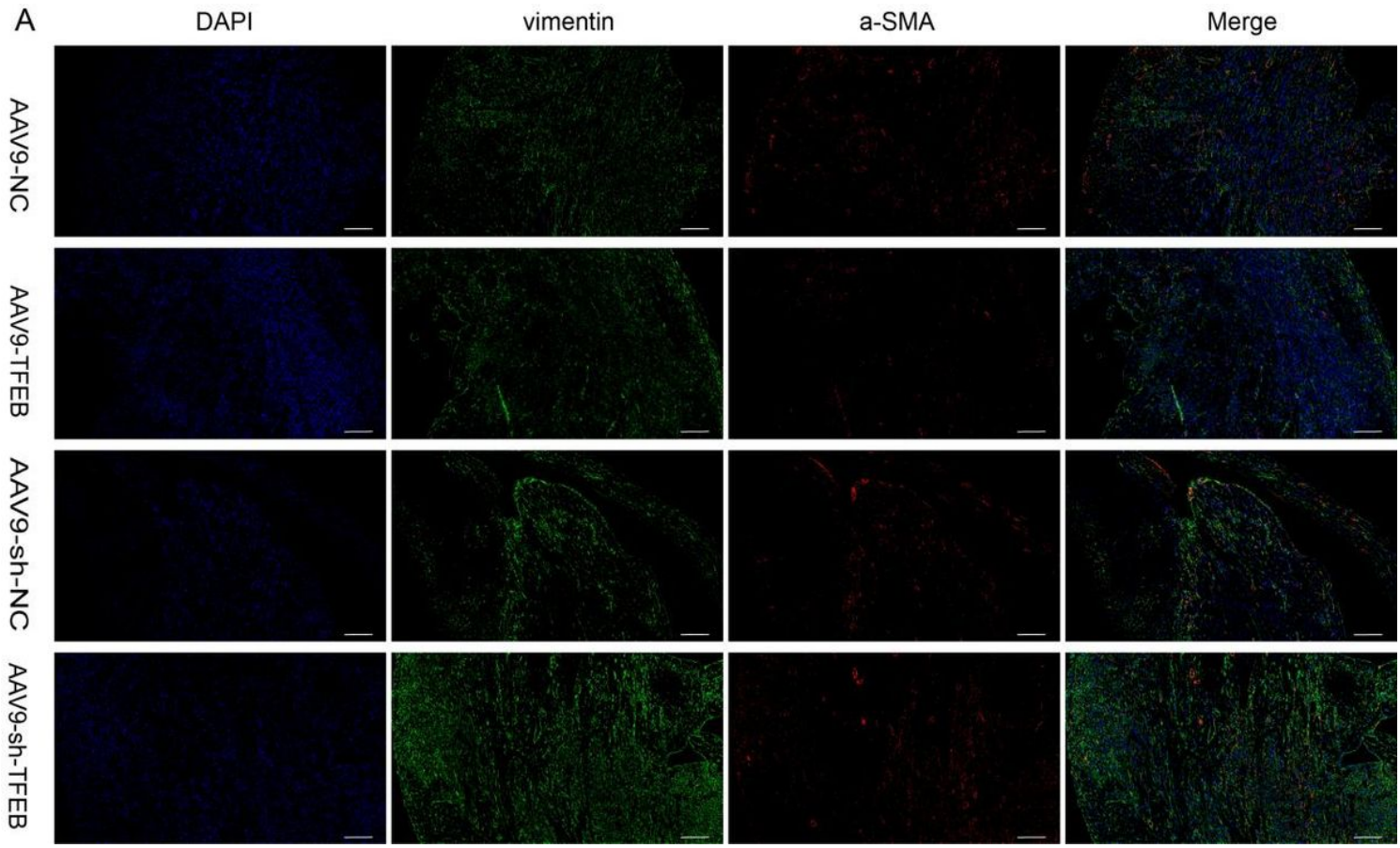

Figure 4

TFEB affected the transformation of fibroblasts three days after MI modeling. (A) Immunofluorescence staining of vimentin (green) and α-SMA (red) of mouse heart three days after MI modeling (10X)(n=3). The picture showed that the MI modeling is successful. Fibroblasts began to proliferate and transform into myofibroblasts. Scale bars represent 100 μm.

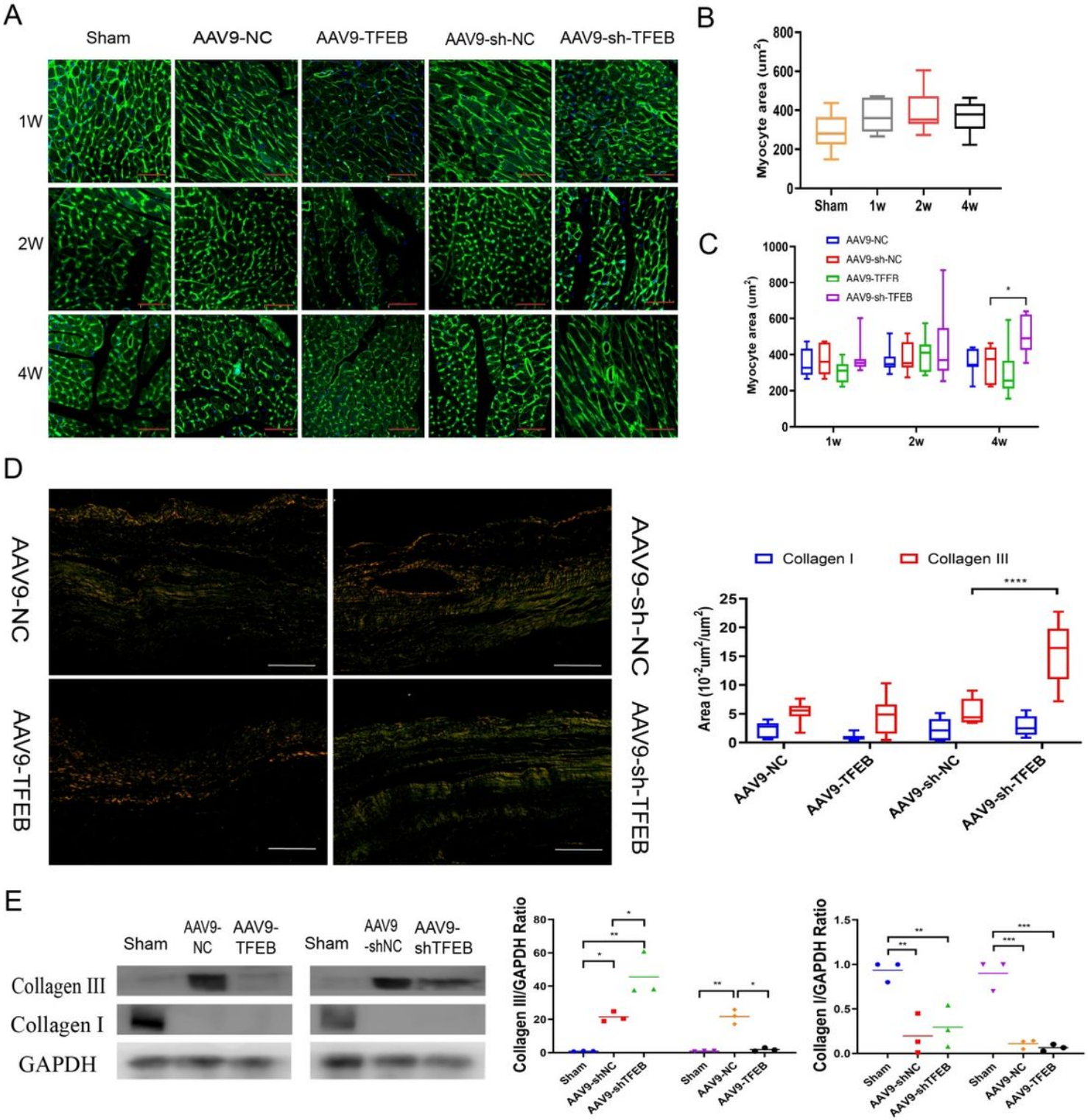

Figure 5

TFEB alleviated myocardial hypertrophy and affected the excretion of ECM four weeks after MI modeling. (A) The myocyte areas stained by the wheat germ agglutinin (WGA). Scale bars represent 50 μm. (B) Myocyte areas at different time points after MI modeling(n=3). (C) Myocyte areas in different groups (qualified from the WGAs staining)(n=3). (D) MI areas stained by Sirius red(n=3). Collagen I was stained into orange and Collagen III was stained into green. Scale bars represent 10 μm. The expression levels of

Collagen I and Collagen III were quantified and presented as mean ± standard deviation (****: $p < 0.0001$). (E) The changes of Collagen I and Collagen III expression were detected using Western blot (*: $p < 0.05$, **: $p < 0.01$, ***: $p < 0.001$)(n=3).

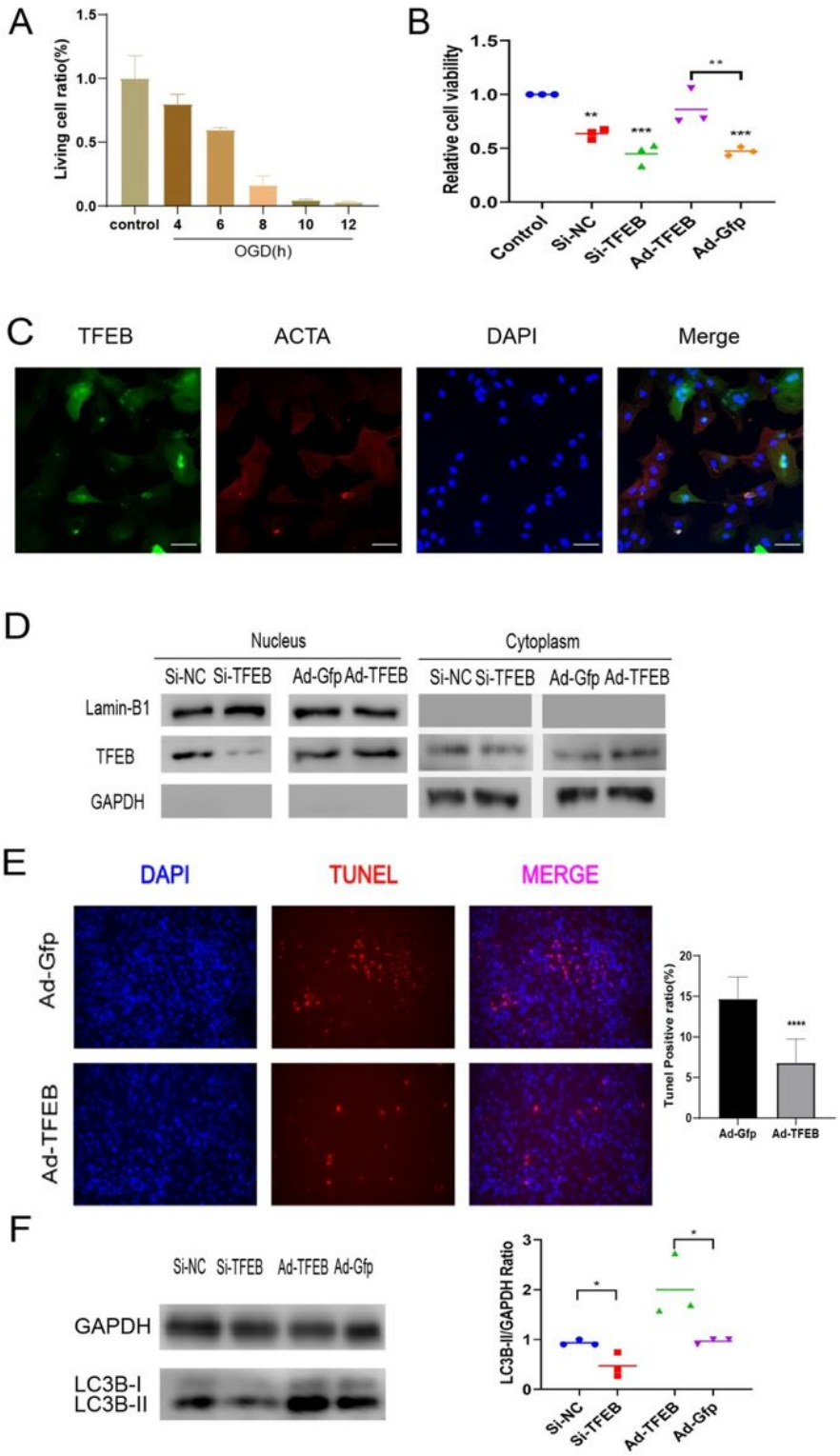

Figure 6

TFEB's impact on Myocardial Autophagy and Apoptosis in OGD Model. (A) OGD time of rat myocardial cells measured by CCK-8 assay. (B) Cell viability of rat myocardial cells six hours after OGD was assessed by CCK-8 assay. (C) TFEB (green) and ACTA (red) were located by Immunofluorescence staining in rat myocardial cells. Scale bars represent 50 mm. (D) TFEB expression in the nucleus and cytoplasm of myocardial cells after OGD. (E) TUNEL staining revealed myocardial cell apoptosis after OGD. (F) The expression of autophagy -related proteins in infarcted areas was detected using Western blotting.

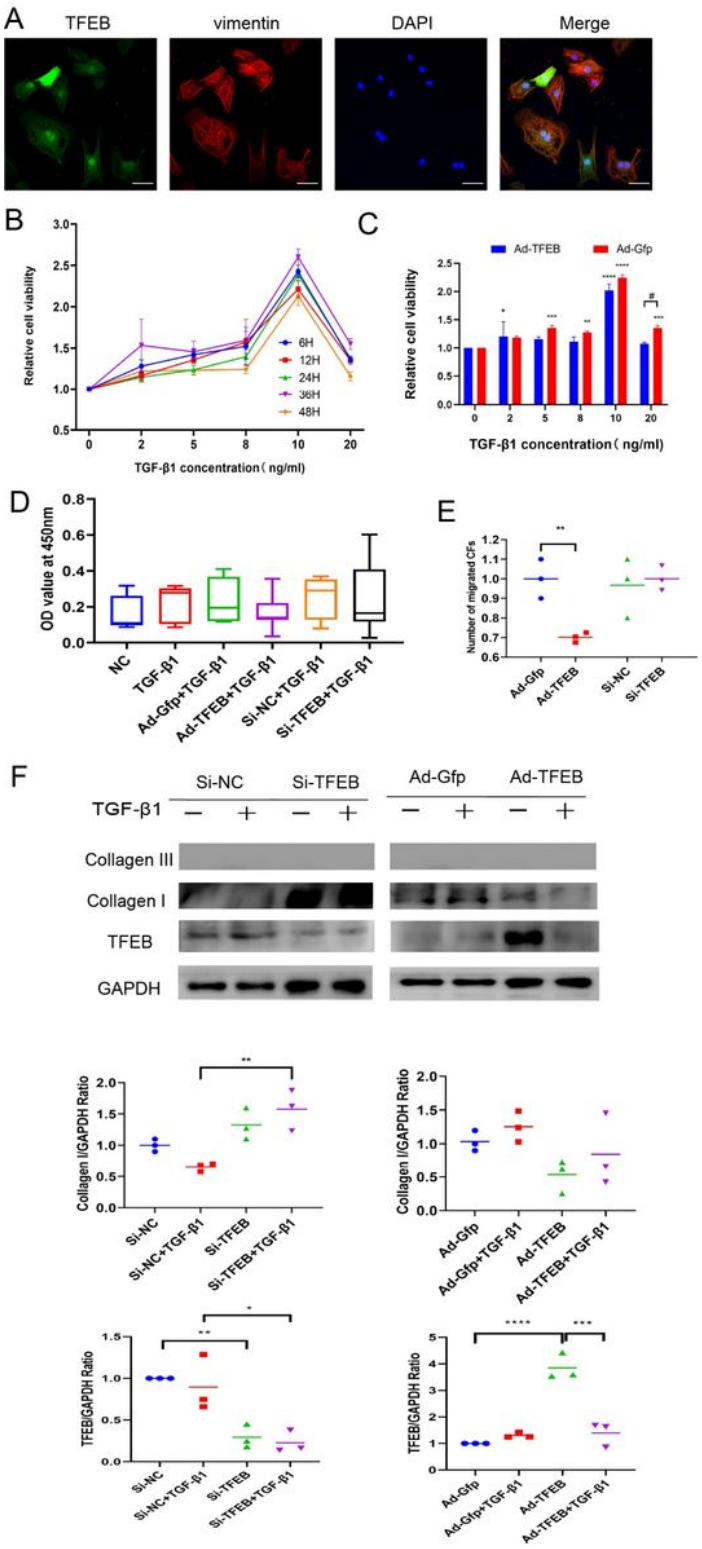

Figure 7

TFEB Affected CFs in Fibrosis model in vitro. (A) Immunofluorescence staining of TFEB (green) and vimentin (red) in rat fibroblasts. (B) Effects of TGF-β1 of different concentrations and incubation time on proliferation of CFs of rats were measured by CCK-8 assay. (C) Cell viability assessed by CCK-8 assay after rat CFs were treated with increasing concentration of TGF-β1 for 12 hours (*: $p < .05$, **: $p < 0.01$, ***: $p < 0.001$, ****: $p < 0.0001$, ##: $p < 0.01$). (D) EDU assay was used to evaluate the influence of TFEB on proliferation of CFs after co-incubated with TGF-β1 (5 ng/ml) for 12 hours. (E) Cell migration was evaluated by the Transwell assay for the unstimulated CFs (control) and the CFs co-incubated with TGF-β1 (5 ng/mL) for 12 hours. (**: $p < 0.01$). (F) The expression difference of Collagen I in CFs detected using Western blot (**: $p < 0.01$).

Supplementary Files

This is a list of supplementary files associated with this preprint. Click to download.

- renamede841d.docx